Neural Comput & Applic (2013) 23:2059–2071
DOI 10.1007/s00521-012-1149-1

ORIGINAL ARTICLE

A computer-aided diagnosis system for malignant melanomas

N. Razmjooy · B. Somayeh Mousavi · Fazlollah Soleymani · M. Hosseini Khotbesara

Received: 28 April 2012 / Accepted: 24 August 2012 / Published online: 6 October 2012

Abstract The aim of this study is to provide an efficient way to segment the malignant melanoma images. This method first eliminates extra hair and scales using edge detection; afterward, it deduces a color image into an intensity image and approximately segments the image by intensity thresholding. Some morphological operations are used to focus on an image area where a melanoma boundary potentially exists and then used to localize the boundary in that area. The distributions of texture and a new feature known as AIBQ features in the next step provide a good discrimination of skin lesions to feature extraction. Finally, we rely on quantitative image analysis to measure a series of candidate attributes hoped to contain enough information to differentiate malignant from benign melanomas. The selected features are applied to a support vector machine to classify the melanomas as malignant or benign. By our approach, we obtained 95 % correct classification of malignant or benign melanoma on real melanoma images.

N. Razmjooy
Young Researchers Club, Majlesi Branch,
Islamic Azad University, Isfahan, Iran

B. Somayeh Mousavi
Young Researchers Club, Zahedan Branch,
Islamic Azad University, Zahedan, Iran

F. Soleymani (✉)
Department of Mathematics, Zahedan Branch,
Islamic Azad University, Zahedan, Iran
e-mail: fazl_soley_bsb@yahoo.com

M. Hosseini Khotbesara
Department of Medicine, Ardabil Branch,
Islamic Azad University, Ardabil, Iran

Keywords Malignant melanoma · Support vector machine · Segmentation · Feature extraction · Texture · ABCD rule · Sequential minimal optimization

1 Introduction

Human skin is a complex surface, with fine-scale geometry, which makes its appearance difficult to model. Also, the conditions under which the skin surface is viewed and illuminated greatly affect its appearance. The skin can easily be examined with the eyes; however, many particular aspects of the skin are better evaluated by noninvasive imaging methods.

Skin cancer is one of the most common and one of the deadliest types of cancer among the fair-skinned population. Among the different types of skin cancer, *melanoma* is the most serious form. If it is recognized and treated early, it is almost always curable, but if it is not, the cancer can advance and spread to other parts of the body, where it becomes hard to treat and can be fatal [1]. Although it is not the most common of the skin cancers, it causes the most deaths. The American Cancer Society [2] estimates that at present, about 120,000 new cases of melanoma in the United States are diagnosed in a year. In 2010, about 68,130 of these were invasive melanomas, with about 38,870 in men and 29, 260 in women. Clinical features of pigmented lesions suggestive of melanoma are known as the ABCD of melanoma [3]: asymmetry, border irregularity, color variegation, and diameter greater than 6 mm. The ABCD criteria developed by the American Cancer Society provide a starting-off point for the physician and an easily remembered guideline for the patient to use in self-examination for MM. Experts, using these symptoms (known as ABCD rule), can recognize the melanoma.

To compute the ABCD score, the criteria are assigned semi-quantitatively. Each of the criteria is then multiplied by a given weight factor to give a total dermoscopy score as an outcome. The ABCD rule works properly for thin melanocytic wounds. These rules have 59–88 % accuracy in diagnosing melanoma, but biopsy is needed for more precise diagnosis [4].

Measurement of image features for diagnosis of melanoma requires that first the lesions be detected and localized in an image. Automated systems for detecting melanoma use one imaging modality (such as dermoscopy), mathematical models, and computer algorithms to predict whether a skin lesion is melanoma [5]. Paul Wighton et al. [6] have improved an automatic method for segmenting skin lesions by leveraging notice exploited from expert ground truth and the random walker algorithm. They utilized color as a texture to perform the segmentation.

Xiang Li et al. [7] developed a local probabilistic approach to segment the lesions from their background. Multivariate Gaussian mixture model is discussed as the way to model the density distribution of properties. They used color, depth, and texture information to produce the best results compared with those of others.

In 2004, Zagrouba and Barhoumi [8], motivated by the desire to classify skin lesion from color images, used a fuzzy classifier after eliminating the noise to classify the images and attained a 79.1 % accuracy for correct classification of lesions.

Density-Based Spatial Clustering of Application with Noise [9] and JSEG [10] are examples of applying clustering algorithms in lesion segmentation.

Zouridakis et al. [11] expanded an automatic skin lesion malignance detection system based on size difference of two image modalities [12]: XLM and TLM. The XLM imaging modality captures only surface pigmentation [13].

In 2011, Fassihi et al. [14] employed coefficients of wavelet decomposition to extract image's features. Melanoma classification was carried out by using the variance and mean of wavelet coefficients of images as the inputs of neural network. Results showed 90 % ability in distinction between benign and malignant lesions.

In this study, first a new simple hair removal based on edge detection is introduced as a pre-processing step; afterward, a new morphology-based technique is described as early detection of a melanoma lesion based on the analysis of a pair of TLM and XLM images, which are used to accurately measure the melanoma characteristics of the lesion that is presented. The next section is dedicated to classification. Finally, our findings are discussed.

Figure 1 shows the workflow of our approach. The system takes a different TLM and XLM image as input and the traced image as input; for preventing some errors, a pre-processing such as hair removal is applied to the system.

2 Materials and methods

Here we describe the employed technique and the instrument used for data acquisition.

2.1 Input dataset

Various lesions from different references (like [2, 5]) are used in this work. It consists of 68 pairs of XLM and TLM images captured by the same Nevoscope device under lighting conditions (notice that to the present purpose, just 40 pairs of melanoma images are used to feature extraction step). The size of all dataset's images was cropped to a spatial resolution of 256 × 256 pixels to reduce the computational resources needed for processing the images.

For some lesions, two distinct images were used: one in the TLM and one in the XLM modality. However, segmentation is difficult because of the wide range of lesion shapes and colors and also different skin tones; Fig. 2 shows these diversities.

2.2 Pre-processing

Before commencing the main processing, a hair removal system is needed to eliminate the extra hairs and scale lines in image for easing the skin melanoma segmentation.

Most of the related works used a method known as *Dull Razor,* and advantages of that are given as follows [15]:

1. It identifies the dark hair locations by a generalized grayscale morphological closing operation,

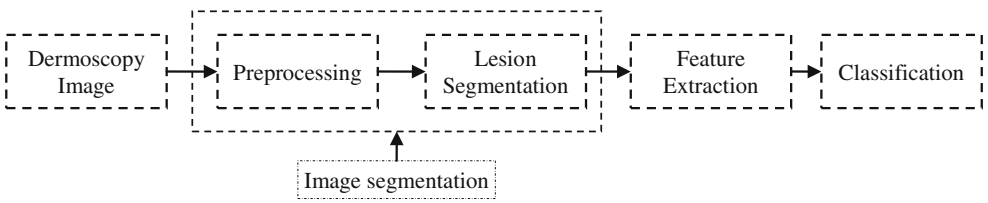

Fig. 1 Flowchart of the designed lesion detects system

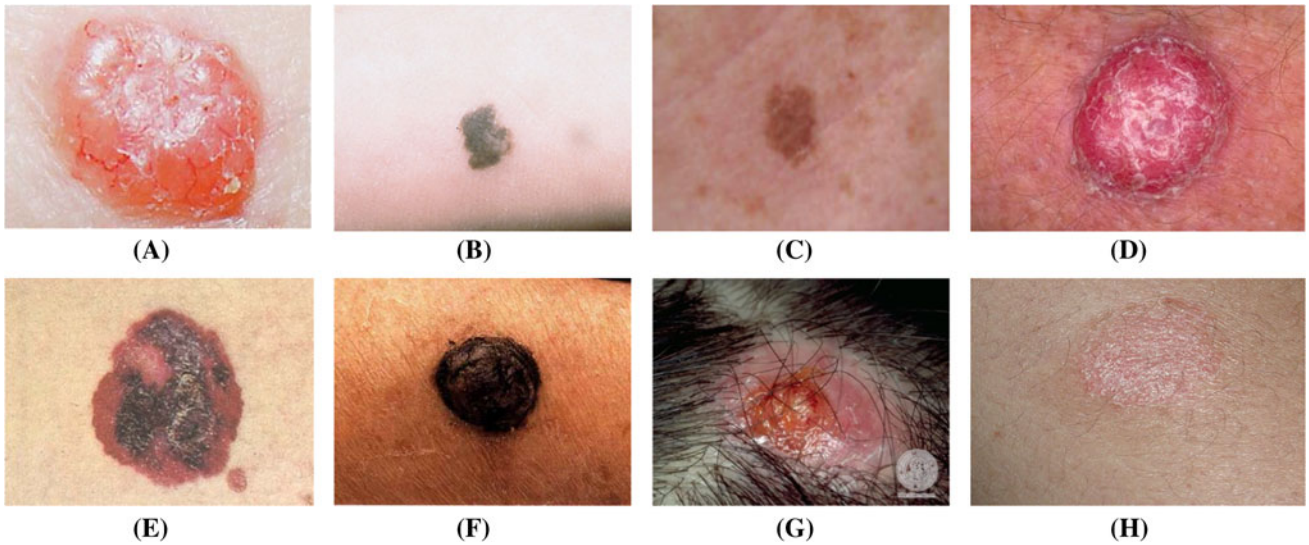

Fig. 2 The diversity of dermoscopy images: **a** basal-cell carcinoma, **b** acral lentiginous, **c** lentigo maligna, **d** squamous cell carcinoma, **e** melanoma superficial spreading, **f** melanoma superficial spreading, **g** sebaceous gland carcinoma, **h** discoid eczema

2. It verifies the shape of the hair pixels as thin and long structure and replaces the verified pixels by a bilinear interpolation, and
3. It smoothes the replaced hair pixels with an adaptive median filter.

In this paper, a new method based on edge detection is employed as below:

2.2.1 *Filtering*

Reduction in over-segmentation is typically carried out by temporal or spatial averaging techniques. Such reduction is a typical pre-processing step to improve the results of later processing (in this paper, edge detection of an image). Median filtering is very widely used in digital image processing because, under certain conditions, it preserves edges while removing over-segmentation. Specifically, the median filter replaces a pixel by the median of all pixels in the neighborhood:

$$y[m,n] = \text{median}\{x[i,j], (i,j) \in \omega\} \quad (1)$$

where ω represents a neighborhood cantered around location (m, n) in the image [16].

The median filter considers each pixel in the image in turn and looks at its nearby neighbors to decide whether or not it is representative of its surroundings. The median is evaluated by first sorting all the pixel values from the surrounding neighborhood into numerical order and then replacing the pixel being considered with the middle pixel value [17].

In this paper, a nonlinear filter assigns to each pixel the median pixel value over a neighborhood of a given size. This filter reduces the effect of small structures, like hair, and scale lines on the segmentation result. The neighborhood used for the median filter depends on the image resolution. In this work, a 9×9 neighborhood has been used for images of size 256×256 pixels showing a complete skin lesion. Trials and errors showed that even if the lesions vary in size, this value can be kept fixed.

2.2.2 *Hair removal*

After smoothing the image, hair removal is done as below:

1. Canny edge detection
2. Thicken morphological operation
3. Dilate morphological operation
4. Add to original image

In this method, thickening operation thickens objects by adding pixels to the exterior of objects until doing so would result in previously unconnected objects being 8-connected. This option preserves the Euler number; like other morphological operators, the behavior of the thickening operation is described by a structure element.

A structure element is a simple, pre-defined shape, represented as a binary image, used to probe another binary image, in morphological operations such as erosion, dilation, opening, and closing.

The binary structure elements employed for thickening are of the verbose type described under the hit-and-miss transform, that is, they can contain both ones and zeros.

The thickening operation is subordinated to the hit-and-miss transform and can be presented quite simply in terms of it. The thickening of an image I by a structuring element J is:

$$\text{THIKEN}(I, J) = I \cup \text{hit-and-miss}\,(I, J), \tag{2}$$

Thus, the thickened image contains the original image adding any additional foreground pixels switched on by the hit-and-miss transform.

Let C and D be two structure elements satisfying $C \cap D = \theta$. The pair (C, D) is often called *composite structuring element*. The hit-or-miss transform of a given image A by $B = (C, D)$ is given by:

$$A \cdot B = (A \Theta C) \cap (A^c \Theta D), \tag{3}$$

where A^c is the set complement of A and Θ is erosion sign.

That is, a point x in E belongs to the hit-or-miss transform output if C translated to x fits in A, and D translated to x misses A (fits the background of A).

And dilate performs dilation using the structuring element (in this work, it is 3×3). Figure 3 illustrates a simple comparison between the usage of the proposed hair removal to lesion segmentation and without it.

2.3 Lesion segmentation

This method is based on mathematical morphology, and the main purpose of this technique is to enhance the edges on the lesion boundary, while suppressing the gradients inside the lesion and in the background. Initial tests with a training set consisting in a subset of 15 randomly selected images showed that because of different colors in various dataset, colors aggravate the results; hence, color images are converted to the intensity mode to get better results. This method consists in the following steps:

1. Transform the color space from RGB to the intensity mode using the equations:

   $$\text{Intensity} = \frac{1}{3}(R + G + B),$$

2. The nonlinear transformation procedure produces a histogram for the smoothed image that is bimodal and has two distinct peaks. Hence, the method by Kapur [18] can be used to automatically threshold the image and obtain a binary mask that represents only the lesion.

The Kapur's method is based on the entropy theory. It consists in the maximization of the class entropies, which is interpreted as a measure of class compactness and accordingly, of class separability. The probability distribution of the gray levels over the black part of the image is:

$$\frac{p_0}{P_B}, \frac{p1}{P_B}, \ldots, \frac{p_s}{P_B}, \tag{4}$$

and white part is:

$$\frac{p_{s+1}}{1 - P_B}, \frac{p_{s+2}}{1 - P_B}, \ldots, \frac{p_{n+1}}{1 - P_B}, \tag{5}$$

where s is the threshold; p_i ($i = 0, 1, \ldots, n - 1$) is the statistical probability of pixels with gray level i in the entire image; P_B is the probability of pixels with gray level less than or equal to threshold s.

$$P_B = \sum_{i=0}^{s} p_i, \tag{6}$$

The entropy of the black part (object) of the image is:

$$H_B^{(S)} = -\sum_{i=0}^{s} \frac{p_i}{P_B} \log_2 \left(\frac{p_i}{P_B} \right) \tag{7}$$

and for the white part is

$$H_W^{(S)} = -\sum_{i=s+1}^{n-1} \frac{p_i}{1 - P_B} \log_2 \left(\frac{p_i}{1 - P_B} \right), \tag{8}$$

The total entropy of the image is then defined as:

$$H_T^{(S)} = H_B^{(S)} + H_W^{(S)}, \tag{9}$$

The threshold s is selected as the one that maximizes $H_T^{(S)}$. The experiment result of Kapur's method for one image is shown in Fig. 4.

3. Perform the morphological operations of closing, bridging, filing, thickening, opening and remove on the binary image to fill in the holes within the lesion and make it homogeneous.
4. Compute the lesion boundary as the set of all nonzero pixels that are connected to at least one zero-valued pixel in the binary image. Remove the spurs from the lesion boundary to get a boundary that is only one pixel thick.

As an example, Fig. 4 shows the various steps needed to segment the lesion (from getting the image to segment it) shown in Fig. 5 using the proposed method.

As it can be seen after image acquisition, boundary smoothing is applied to eliminate the noise, scale lines, and even some parts of hairs on the lesion; after that, morphological operations containing thickening and dilating in trailing of edge detection characterize the hair sections; helping this system, hairs on the lesion are neglected and the second step begins; in this step, using a threshold and

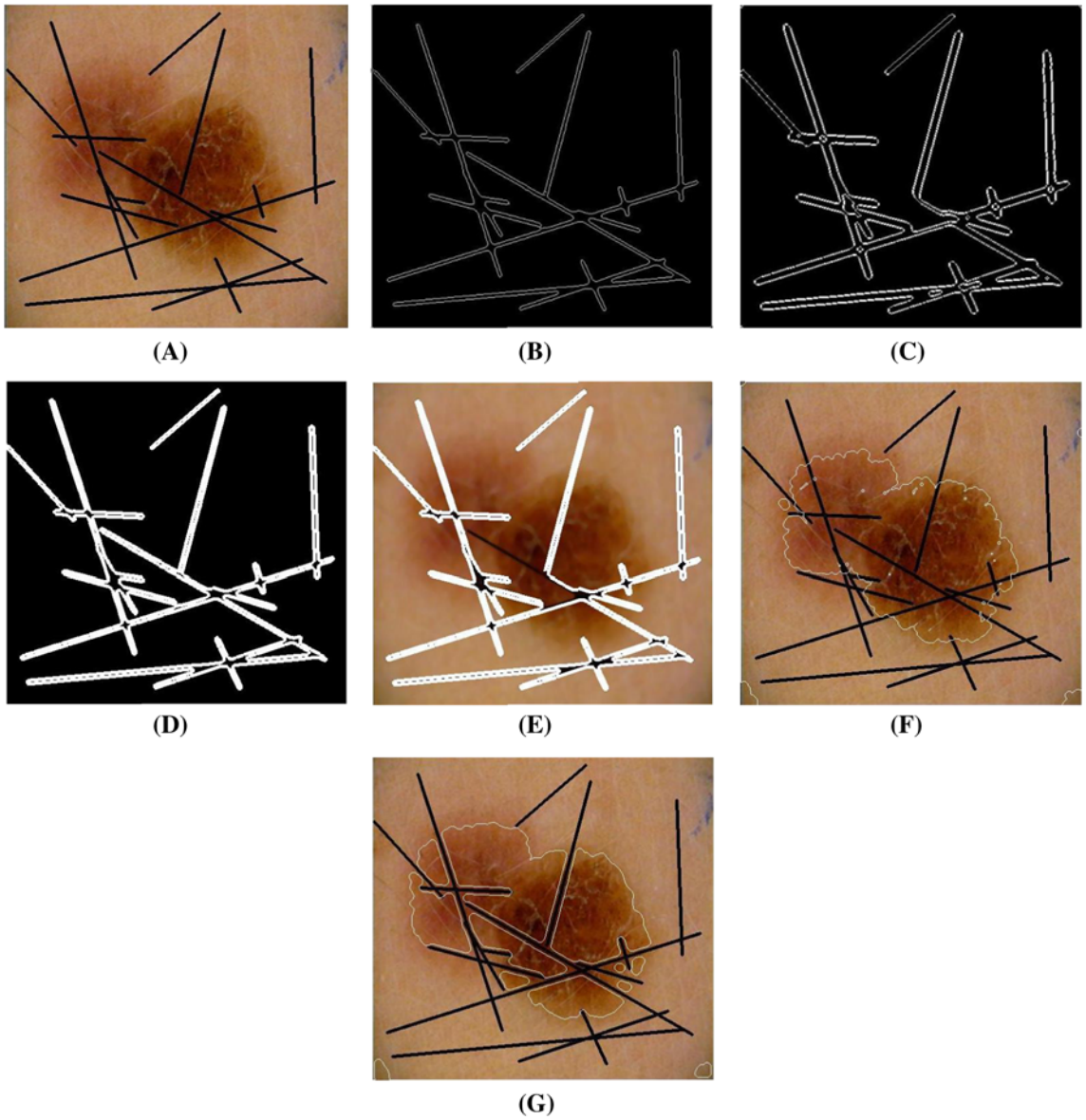

Fig. 3 Result of lesion segmentation using the proposed hair removal method: **a** original image, **b** edged image, **c** thickening of the edged image, **d** and dilating the thickened image, **e** apply whole method to the original image, **f** traced image before and **g** after hair removal

morphological operations consist of closing (for smoothing, fusing narrow breaks, and long thin gulfs, eliminating small holes, and filling gaps in the contour), bridge (bridges unconnected pixels), fill (fills isolated interior pixels), thicken (thickens objects by adding pixels to the exterior of objects until doing so would result in previously unconnected objects being 8-connected), a lesion mask is detected; finally, adding border drawing to the original image shows the lesion boundary.

2.4 Lesion feature description

The significant problem in automatic melanoma detection is to find relevant and proper properties describing malignant lesions in order to ensure the isolation between melanoma malignant and benign lesions, particularly, informal benign lesions that may be clinically mistaken for melanoma. ABCD rules are used to have an accurate system in recognition part; if the mole or growth has one or more of the ABCD, it should be shown to a physician as soon as possible (Fig. 6).

ABCD rules are summarized below:

1. Asymmetry

One half is different than the other half. In other words, asymmetry can be assessed by comparing one half of the growth to the other half to determine whether the halves are

equal in size. The mole, birthmark, or other type of blemish anywhere on your skin is not symmetric (same on both sides).

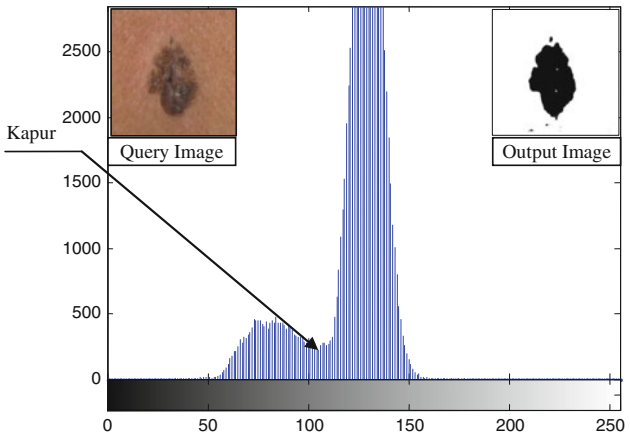

Fig. 4 Experimental results on the gray scale image of a lesion with Kapur's algorithms; input image is in the *left hand*, and histogram of the image is in the *middle* and the output image which is Kapur's threshold after converting to the intensity mode is shown in the *right hand*; threshold = 115

2. Border irregularity

The edges are notched, uneven, or blurred. In other words, if the mole's border is irregular, notched, scalloped, or indistinct, it is more likely to be cancerous (or precancerous) and is thus suspicious.

3. Color

The color is uneven. Shades of brown, tan, and black are present. In other words, variation of color (e.g., more than one color or shade) within a mole is a suspicious finding. Different shades of browns, blues, reds, whites, and blacks are all concerning.

4. Diameter

Diameter is greater than 6 millimeters. In other words, any mole that has a diameter larger than a pencil's eraser in size (>6 mm) should be considered suspicious. Figure 7 shows an example of ABCD rules.

ABCD rules are usually used by dermatologists. Diagnosis by dermatologists based on visual and quantitative

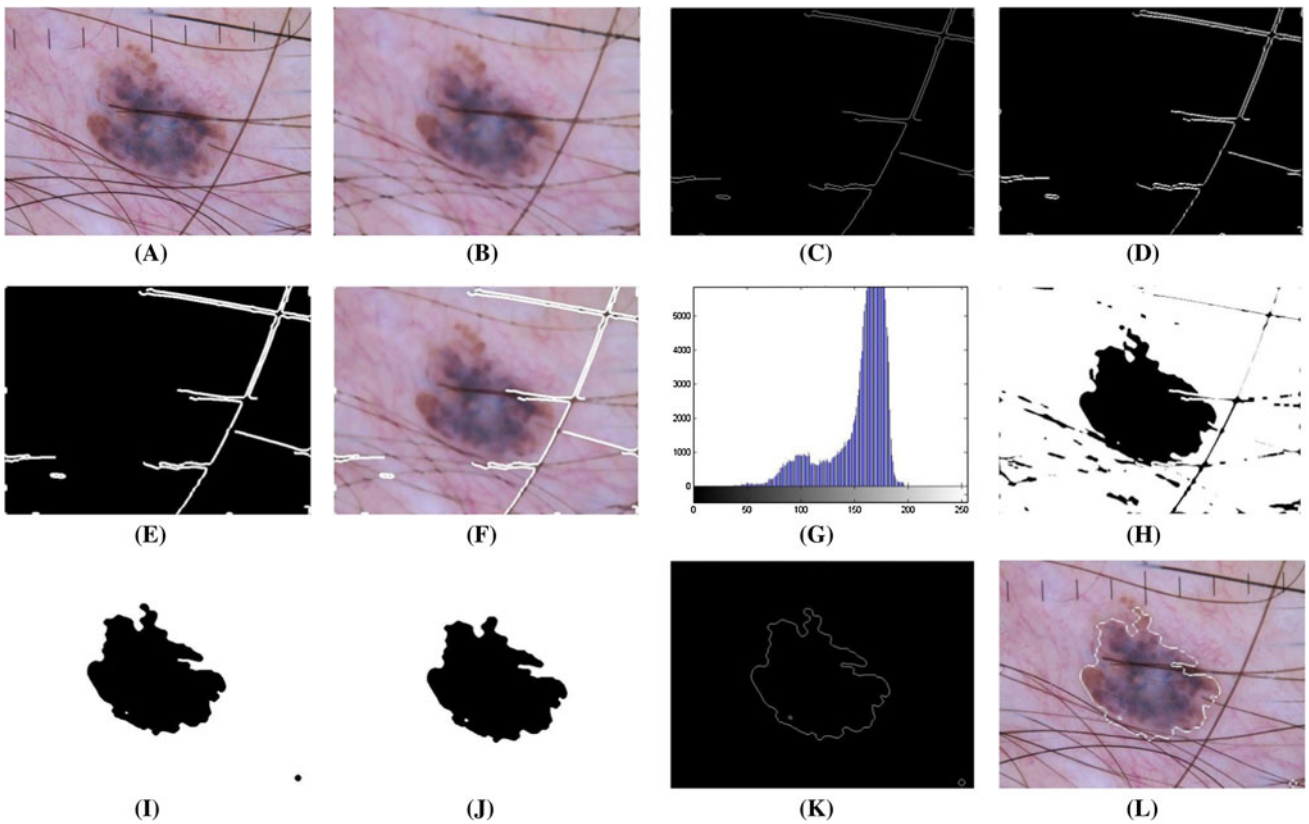

Fig. 5 Various steps implementing method I on the image: **a** input image; **b** image after boundary smoothing; **c** edged image; **d** thickening of **c**; **e** dilating of **d**; **f** apply **e** to the original image; **g** image intensity histogram; **h** apply Kapur's thresholding to **g** after intensity conversion; **i** closing of **h**; **j** opening, bridging, filling, and thickening of **i**; **k** lesion mask; **l** lesion boundary

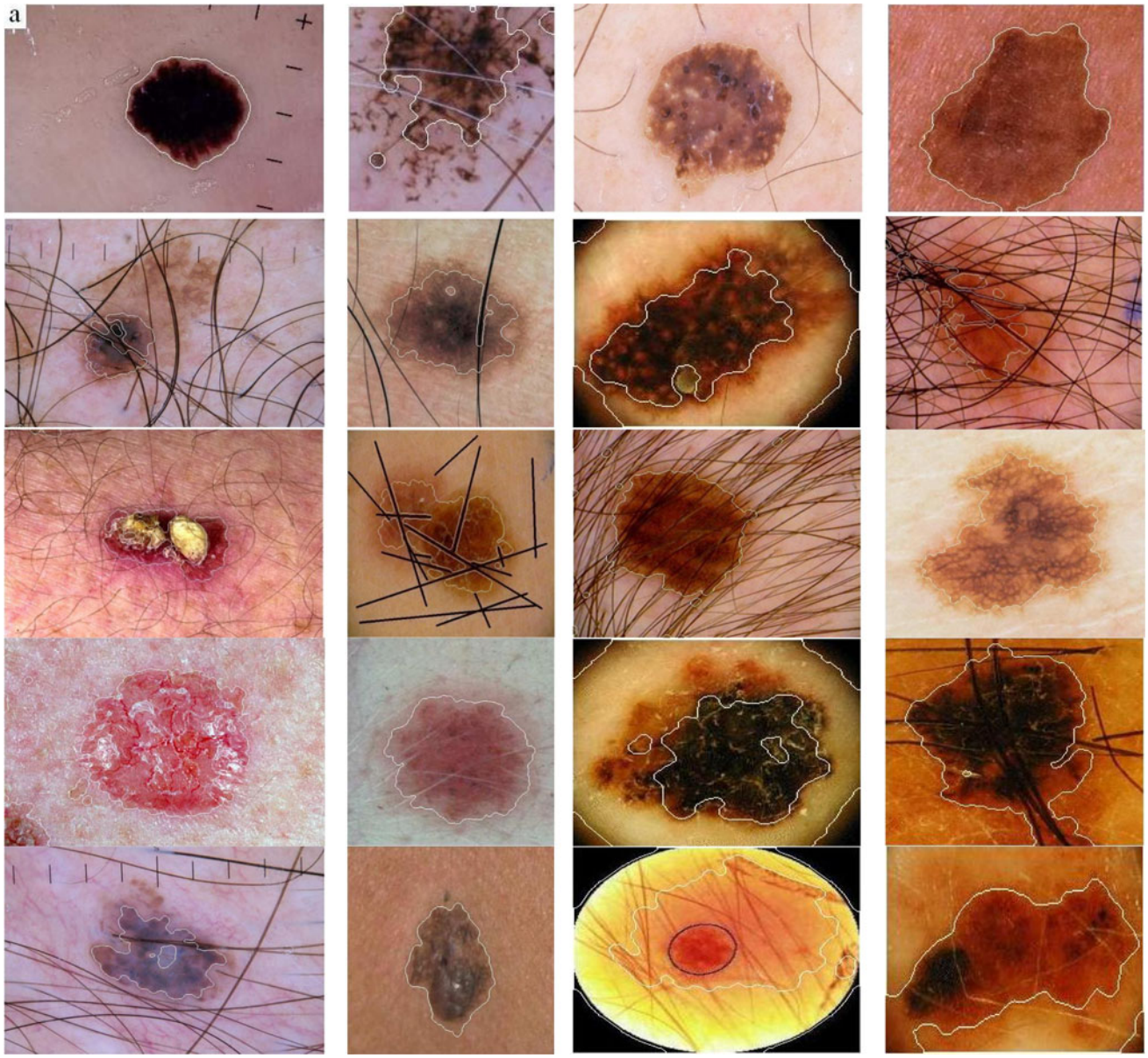

Fig. 6 Some results of lesion segmentation

evolution of such paragon is still may be sensible. So the main purpose of this section is to characterize the ABCD paragon by quantitative properties measured by machine vision and using it as the input of an automated classifier.

In the literature, many features have been used to describe ABCD paragons; as an example in [19], 14 parameters are described but this number of features incremented the classification complexity and elapsed time for the system.

2.4.1 Asymmetry and irregular border quantification (AIBQ)

Asymmetry and irregular (2 types of melanoma malignant sign) border are almost the same; typically none of them have a definitive shape, whereas a benign melanoma has basically a regular shape between circle and oval; therefore, in order to measure these two features, we rely hereafter on a simple algorithm as below:

1. Input segmented image
2. Convert to the binary mode (with Kapur's thresholding)
3. Morphological opening to eliminate the noise and extra information
4. Finding the similarity of lesion to the oval shape rather than circle shape is achieved by implementing a threshold on a defined metric as below:

$$\text{Metric} = \frac{4 \times \pi \times \text{Area}}{\text{Perimeter}^2};$$

5. where *Area* and *Perimeter* are depends on the given shape. Threshold point is empirically achieved as 0.9 (i.e. the values less than or equal to 0.9 are oval). The rotation and labeling operations are ready in the Matlab software [19].
6. If the shape of lesion is similar to oval:

   Find degree of rotation

   Rotate the image in a Reverse angle which is attained in (3)

   End;
7. Label the image result from (3) or (4)
8. α=Find the ratio of the shape rather than the total label surface.
9. If 1.124<α<1.28

   The shape is almost regular and symmetry

   Else

   The shape is abnormal

   End;

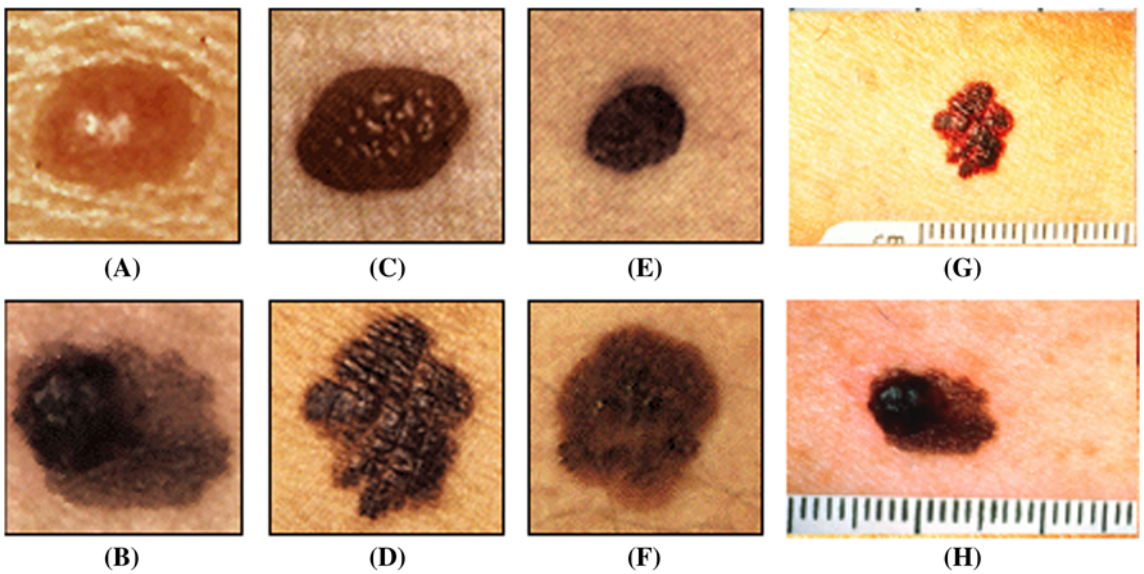

Fig. 7 ABCD rules: **a** symmetric (normal) and **b** asymmetric, **c** regular border (normal) and **d** irregular border, **e** one color (normal) and **f** color variance, **g** similar than 6 millimeter and **h** larger than 6 millimeter

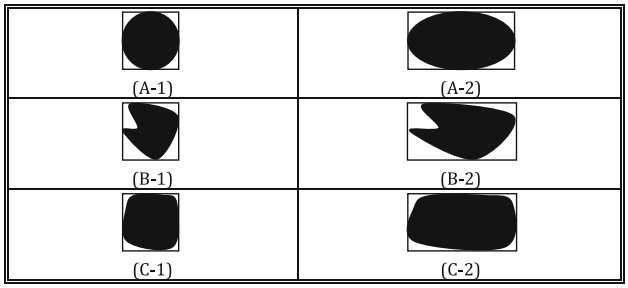

Fig. 8 Different modes of *circle* and *oval shape* of the lesions are shown above; **a** is a normal mode and shows a benign mode of melanoma, but **b** and **c** are two abnormal shapes for the melanoma (malignant melanoma)

If the surface ratio computes to the given 6 shapes (Fig. 8), we have then:

$$\text{For (A-1)} \quad \frac{S_{\text{label}}}{S_{\text{circle}}} = \frac{4rr}{\pi r^2} = \frac{4}{\pi} = 1.2732 = \alpha, \quad r = \text{circle\_radius} \tag{10}$$

$$\text{For (A-2)} \quad \frac{S_{\text{label}}}{S_{\text{oval}}} = \frac{4ab}{\pi ab} = \frac{4}{\pi} = 1.2732 = \alpha. \quad a, b : \text{length, and, height, of, oval} \tag{11}$$

$$\text{For (B-1)} \quad \frac{S_{\text{label}}}{S_{\text{circle}}} < \alpha \tag{12}$$

$$\text{For (B-2)} \quad \frac{S_{\text{label}}}{S_{\text{oval}}} < \alpha \tag{13}$$

$$\text{For (C-1)} \quad \frac{S_{\text{label}}}{S_{\text{circle}}} > \alpha \tag{14}$$

$$\text{For (C-2)} \quad \frac{S_{\text{label}}}{S_{\text{oval}}} > \alpha \tag{15}$$

From the above, it is apparent that the regular and symmetry melanomas (benign melanomas) have a ratio near to 1.2732 (it is no different between oval, circle, and among these two) and the other ratios, which have rather less or more value, show a malignant melanoma; four real examples of implementation of this method are shown in Fig. 9.

In this example, A and B series have almost a circle like shape; therefore, no angle rotation is need to them, whereas C and D series have almost an oval like shape, and whereof oval shapes have always a specific angle from the sheet, a reverse angle rotation in order to the AIBQ technique that affects them (C has a −24.8266 angle and D has a 58.7577 from the sheet).

2.4.2 Statistical color variance quantification

One of the significant approaches to describe a region is to quantify its texture content. An approach employed frequently for texture analysis is based on statistical features of the intensity histogram [20].

The gray scale-based features proposed in this paper to detect color variance are based on texture and are computed from intensity matrices. Those properties are statistical measures extracted from a matrix that performs the relationship between pixels within the region. To describe potato texture, the following measures were chosen as features, where:

$$\text{Mean:} \quad m = \sum_{i=0}^{L-1} z_i P(z_i) \tag{16}$$

Standard deviation:

$$\sigma = \sqrt{\mu_2} = \sqrt{\sum_{i=0}^{L-1} (z_i - m)^2 p(z_i)} = \sqrt{\sigma^2} \tag{17}$$

$$\text{Smoothness:} \quad R = 1 - 1/(1 + \sigma^2) \tag{18}$$

$$\text{Third moment:} \quad \mu_3 = \sum_{i=0}^{L-1} (z_i - m)^3 p(z_i) \tag{19}$$

$$\text{Uniformity:} \quad U = \sum_{i=1}^{L-1} p^2(z_i) \tag{20}$$

$$\text{Entropy:} \quad e = -\sum_{i=0}^{L-1} p(z_i) \log_2 p(z_i) \tag{21}$$

where z is a random variable pointing intensity, $p(z)$ is the histogram of the intensity levels in a region and L is the number of possible intensity levels.

In these features, mean is a measure of average intensity, standard deviation is a measure of average contrast, smoothness measures the relative smoothness of the intensity in a region (R is 0 for a region of constant intensity and approaches 1 for regions with large executions in the values of the intensity levels), third moment measures the skewness of a histogram (this measure is 0 for symmetric histograms; positive by histograms skewed to the right about the mean; and negative for histograms skewed to the left), uniformity measure is maximum when all intensities are equal (from values), and entropy is a measure of randomness. Table 1 shows a sample of using these features for malignant (color variance) textures.

2.4.3 Diameter quantification

A proper algorithm to calculate the diameter is described below:

1. Image acquisition
2. Hair removal
3. Convert to the binary mode using Kapur's method
4. Morphological bridging (to bridge the segregated areas), closing (to eliminate the noise), and filling (to filling the holes) [20].

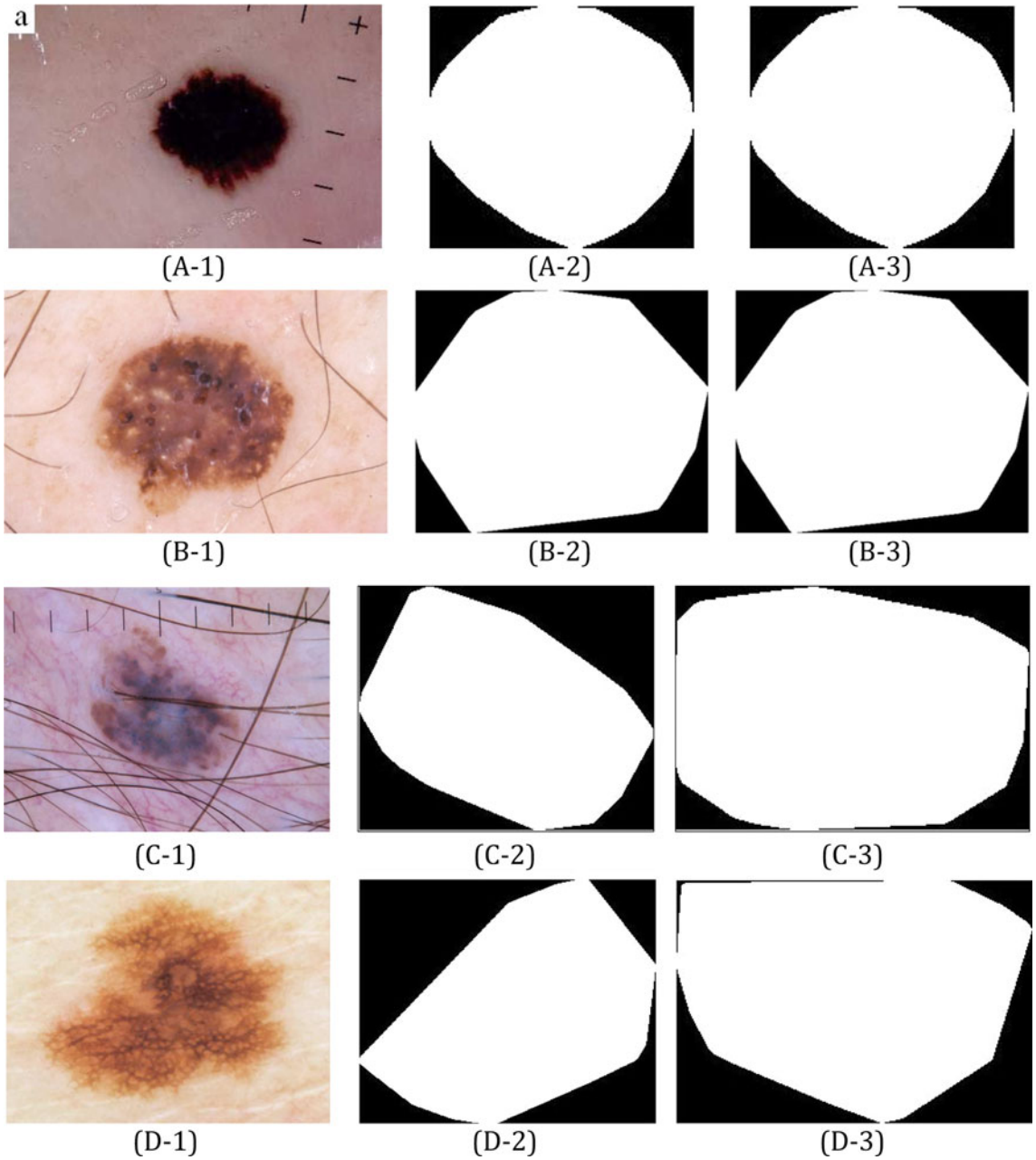

Fig. 9 AIBQ implementation: **A-1**, **B-1**, and **C-1** input image; **A-2**, **B-2**, and **C-2** binary detected lesion; **A-3**, **B-3**, and **C-3** image inverse rotation

Table 1 Texture measures for the given two malignant and benign melanomas from Fig. 6

Texture	Mean	Standard deviation	Smoothness	Third moment	Uniformity	Entropy
Malignant (color variance)—Fig. 6f	77.0812	41.3288	0.0256	1.0266	0.0077	7.2705
Benign (one color)—Fig. 6e	3.8591	2.6691	0.0001	0.0010	0.2533	2.5668

5. Finding the maximum pixels using a simple projection in 4 directions.
6. Finding the diameter in respect to the height of capturing.

In this method, first, the column and row (or oblique) lines that have the most pixels are characterized as the diameter of the image. Figure 10 shows a simple pixel projection to find the pixel diameter.

Fig. 10 Size projected image: **a** input image, **b** binarized image after morphological operations, **c** pixel diameter

After that, it is time to find the real diameter of the image. This projection algorithm uses an approach that can notice horizontal, vertical, and oblique edges. In this technique, we specified the rate of black and white pixels of the binarized image in four directions; after analyzing the results, it could be considered that the system has some numbers for vertical and some for horizontal which comprise the maximum and minimum lines. The whole maximum lines are equal. In this situation, an appropriate precision for proper ratio finding is defined. Maximum diameter, unless otherwise specified, shall not be more than 6 mm in diameter; for this, a standard ratio between size and number of pixels in the image is needed. In respect to various distance levels for capturing image from different datasets (for malignant melanoma), we decided not to use the melanoma diameter ($x < 6$ mm). The vision system of diameter measurement is shown in Fig. 11.

2.5 Support vector machines

Support vector machines (SVMs) will in theory give a better result than using only thresholds for each channel as the network also takes into account the relationship between the channels [21]. Support vector machines are very popular for separate roles because they can precisely synthesize a lot of features to find an optimal separating hyperplane. SVMs minimize the classification error rate based on two qualifications contemporary [22]. They both seek a hyperplane with a major margin, that is, the distance from the nearest sample for segregating hyperplane, and minimize the number of false classified training samples, using slack variables [22]. If a sample is wholly classifiable in feature space, then the second constraint is not necessary [22]. Albeit this is not the case in our outcome, SVMs both minimize the error on the training set and maximize the margin, increasing their generalization ability [23].

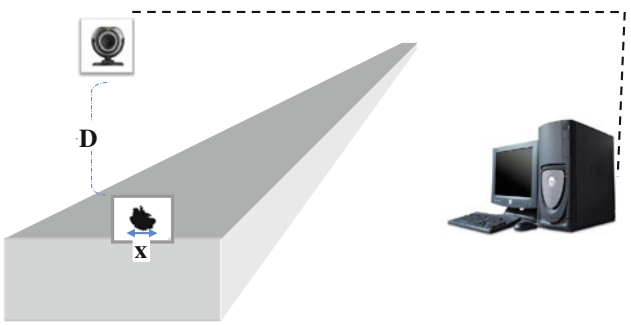

Fig. 11 The computer vision system developed to detect the diameter

SVMs utilize the consequences of statistical learning and optimization theories in order to maximize their generalization authority for samples. These features show that SVMs could develop the performance on malignant melanoma classification [22]. Main idea is to find a decision surface that *best* classifies the data points into two classes. The decision function in SVM is shown below:

$$y = \operatorname{sgn}\left(\sum_{i=1}^{N} y_i \alpha_i K(x, x_i) + b\right) \tag{22}$$

where x is the d-dimensional vector of a test example, $y \in \{-1, 1\}$ is a class label, x_i is the vector for the ith training example, N is the number of training examples, $K(x, x_i)$ is a kernel function, and $\alpha = \{\alpha_1, \ldots, \alpha_N\}$ and b are the parameters of the model. α_i can be leaded from [24]. To have a better result, *Sequential Minimal Optimization* (SMO) is used in this work; SMO is a new SVM learning algorithm, which is conceptually simple, easy to implement, often faster, and has better scaling properties than a standard SVM algorithm [21]. SVMs are starting to impart increasing adoption in the machine learning communities, but two major weaknesses of it limited its use by engineers. First, the training of SVM is slow, especially for large problems [22]. Second, SVM training algorithms are complex, tenuous, and sometimes difficult to implement. The *quadratic programming* (QP) problem to train an SVM is shown below: we need to find suitable Lagrange; multipliers α_i to get the following function reaches its maximum value [22].

$$\operatorname{Max} W(\alpha) = \sum_{i=1}^{n} \alpha_i - \frac{1}{2} \sum_{i=1}^{n} \sum_{j=1}^{n} y_i y_j k(x_i, x_j) \alpha_i \alpha_j, \quad \forall i, 0 \le \alpha_i \le C \tag{23}$$

Subject to

$$\sum_{i=1}^{n} y_i \alpha_i = 0 \tag{24}$$

Unlike standard SVM learning algorithms, which use numerical quadratic programming as an inner loop, SMO uses an analytic QP step [22] because SMO expends most of the elapsed time to evaluate the decision function instead of QP performing [22]. In such condition, a point is an optimal point if and only if the KKT (Karush-Kuhn-Tucker) conditions are fulfilled. The KKT conditions can be shown as follows:

$$\alpha_i = 0 \Rightarrow y_i f(x_i) \geq 1 \tag{25}$$

$$0 \leq \alpha_i \leq C \Rightarrow y_i f(x_i) = 1 \tag{26}$$

$$\alpha_i = C \Rightarrow y_i f(x_i) \leq 1 \tag{27}$$

The KKT conditions can be measured as one example for one Lagrange multiplier once, which is useful in the structure of the SMO algorithm [22]. At every step, SMO selects two Lagrange multipliers to jointly optimize (using KKT condition above), finds the optimal values for these multipliers, and updates the SVM to reflect the new optimal contents. The prominence of SMO lies in the fact that solving for two Lagrange multipliers can be done analytically [21]. An entire inner iteration due to numerical QP optimization is eluded. In addition, SMO does not need sorely matrix memory (to store previous α_1 α_2 and current α_1 α_2, we only need 2×2 matrices). Thereupon, very large SVM training issues can fit inside of the memory of a personal computer. The two Lagrange multipliers must fulfill all of the qualifications of the main issue. The inequality constraints motivate the Lagrange multipliers to lie in the box. Hence, one step of SMO must find an optimum of the cost function on a diagonal line segment [22]. Some features used for classification are presented in Tables 2 and 3.

Table 4 Classification accuracy results using the training and testing selected dataset

	CDR	FAR	FRR
Train (%)	97.5	1.5	1
Test (%)	95	3	2

2.6 Apply classification

A two-module classification (as benign or malignant individually) is employed in this paper; we discuss *pixel-based* melanoma detection classifiers, which classify each pixel, independently from its neighbors. SVM has been applied to different applications such as texture classification, as in [21–23]. In this paper, we used Sequential Minimal Optimization and parameters are as: C (optimal parameter) is equal to 100, and end-accuracy is 10^{-4}.

To assess the performance of the proposed classifier, three performance metrics are described. First metric is the

Table 2 Seven sample features described malignant melanoma

Mean	Standard deviation	Smoothness	Third moment	Uniformity	Entropy	AIBQ
99.6373	27.5240	0.0115	−0.1103	0.0110	6.7193	1.23
79.5967	35.3511	0.0189	0.3612	0.0082	7.1311	1.29
57.6457	18.9809	0.0055	0.0876	0.0176	6.1069	1.43
112.6461	23.0513	0.0081	0.1071	0.0130	6.5136	1.34
56.4595	29.9090	0.0136	0.1269	0.0100	6.7783	1.74
54.5123	13.4714	0.0028	0.0007	0.0225	5.7508	1.32
100.8243	25.6973	0.0101	−0.0806	0.0118	6.6123	1.91

Table 3 Seven sample features described benign melanoma

Mean	Standard deviation	Smoothness	Third moment	Uniformity	Entropy	AIBQ
3.8591	2.6691	0.0001	0.0010	0.2533	2.5668	1.23
133.1667	10.2149	0.0016	−0.0044	0.0329	5.1214	1.22
74.1111	5.3092	0.0004	0.0029	0.0686	4.1267	1.25
103.5000	7.5860	0.0009	−0.0053	0.0469	4.7111	1.24
49.3673	5.8141	0.0005	0.0028	0.0658	4.2014	1.27
67.2842	9.4353	0.0014	0.0130	0.0356	5.0676	1.25
80.2837	10.1546	0.0016	0.0159	0.0362	5.1035	1.26

correct detection rate (CDR) and is given in Eq. 28. The false acceptance rate (FAR) is the percentage of identification moments in which false acceptance occurs. The false rejection rate (FRR) is the percentage of identification moments in which false rejection occurs. The FAR and FRR are expressed in Eqs. 28 and 29, respectively (Table 4).

$$\text{CDR} = \frac{\text{no of pixels correctly classified}}{\text{total pixels in the test dataset}} \quad (28)$$

$$\text{FAR} = \frac{\text{no of non} - \text{skin pixels classified as skin pixels classified}}{\text{total pixels in the test dataset}} \quad (29)$$

$$\text{FRR} = \frac{\text{no of skin pixels classified as non} - \text{skin pixels classified}}{\text{total pixels in the test dataset}} \quad (30)$$

3 Conclusion

This paper presented an algorithm to develop the diagnoses of malignant melanoma using image processing and machine vision. This algorithm consisted of pre-processing to eliminate hair and scale lines, image segmentation, feature extraction and classification. The results showed 95 % accuracy, 3 % FAR, and 2 % FAR. The first point is a suitable dataset based on specific condition and device to construct a suitable pre-processing step. In the second step, some statistical measures on the texture and a new feature as AIBQ are applied to texture feature extraction of the segmented images and select more suitable features by the use of ABCD rules.

References

1. Detmar M (2000) Tumor angiogenesis. J Investig Dermatol Symp Proc 5:20–23
2. http://www.cancer.org/index
3. Ng VTY, Fung BYM, Lee TK (2005) Determining the asymmetry of skin lesion with fuzzy borders. Comput Biol Med 35:103–120
4. Patwardhan SV, Dai S, Dhawan AP (2005) Multispectral image analysis and classification of melanoma using fuzzy membership based partitions. Comput Med Imaging Graph 29:287–296 (elsevier)
5. Ganster H, Pinz A, Rohrer R, Wildling E, Binder M, Kittler H (2001) Automated melanoma recognition. IEEE Trans Medical Imaging 20(3):233–239
6. Wighton P, Sadeghi M, Lee TK, Atkins MS (2009) A fully automatic random walker segmentation for skin lesions in a supervised setting. In: MICCAI '09 proceedings of the 12th international conference on medical image computing and computer-assisted intervention: part II, pp 1108–1115
7. Li X, Aldridge B, Ballerini L, Fisher B, Rees J (2009) Depth data improves skin lesion segmentation. In: MICCAI '09 proceedings of the 12th international conference on medical image computing and computer-assisted intervention: part II, pp 1100–1107
8. Zagrouba E, Barhoumi W (2004) A preliminary approach for the automated recognition of malignant melanoma. Image Anal Stereol 23:121–135
9. Celebi ME, Aslandogan YA, Bergstresser PR (2005) Mining biomedical images with density-based clustering. In: International conference on information technology: coding and computing, ITCC 2005, Proceedings, IEEE
10. Celebi ME, Aslandogan YA, Bergstresser PR (2005) Unsupervised border detection of skin lesion images. In: International conference on information technology: coding and computing, ITCC 2005, Proceedings, IEEE
11. Doshi M (2004) Automated segmentation of skin cancer images. Master's thesis, University of Houston (May 2004)
12. Nevoscope, http://www.nevoscope.com
13. Binder M (2000) Skin examination device, US Patent Number 6,032,071
14. Fassihi N, Shanbehzadeh J, Sarafzadeh A, Ghasemi E (2011) Melanoma diagnosis by the use of wavelet analysis based on morphological operators. In: Proceedings of the international multiconference of engineers and computer scientists 2011, 16–18 March 2011, Hong Kong, vol 1, pp 193–196
15. Bayro-Corrochano E, Eklundh J-O (2009) Pigmented skin lesions classification using dermatoscopic images. In: CIARP 2009, LNCS, vol 5856. Springer, Berlin, pp 537–544
16. http://fourier.eng.hmc.edu/e161/lectures/smooth_sharpen/node3.html
17. Davies E (2005) Machine vision theory, algorithms and practicalities (signal processing and its applications). ISBN: 0122060938, Morgan Kaufmann, USA
18. Kapur JN, Sahoo PK, Wong AKC (1985) A new method for gray level picture thresholding using the entropy of the histogram. Comput Vis Graph Image Process 29:273–285
19. Zagrouba E, Barhoumi W (2003) Objective and cost-efficient approach for skin lesions classification. In: Proceeding of the IEEE/ACS international conference on computer systems and applications, vol 6. Gammarth, Tunisia, pp 135–150
20. Gonzalez RC, Woods RE, Eddies SL (2009) Digital image processing using MATLAB, 2nd edn. Gatesmark Publishing, Knoxville
21. Brereton RG, Lloyd GR (2010) Support vector machines for classification and regression. Analyst 135(2):230–267
22. Razmjooy N, Mousavi BS, Soleymani F (2012) A real-time mathematical computer method for potato inspection using machine vision". Comput Math Appl 63:268–279
23. Hsu C-W, Chang C-C, Lin C-J (2003) A practical guide to support vector classification. Technical report, Department of Computer Science, National Taiwan University, July 2003
24. Kim KI, Jung K, Park SH, Kim HJ (2003) Support vector machines for texture classification. IEEE Trans Pattern Anal Mach Intell 24(11):1542–1550